Journal of Science Engineering Technology and Management Science *ISSN: 3049-0952*
Volume 03, Issue 03, March 2026 *www.jsetms.com*

RESTORATION OF MARKER OCCLUDED HEMATOXYLIN AND EOSIN-STAINED WHOLE SLIDE HISTOLOGY IMAGES USING GENERATIVE ADVERSARIAL NETWORKS

[1]Mr Sarma Adithe, [2]Ch.Sharmila, [3]K. Kusuma, [4]S. Yamuna Devi, [5]G. Roja
[1]Associate professor, Dept of E.C.E, BVCITS, Batlapalem, Amalapuram, AP
[2,3,4,5]B. Tech, Dept of E.C.E, BVCITS, Batlapalem, Amalapuram, AP

Submitted: 11-02-2026 *Accepted: 18-03-2026* *Published: 24-03-2026*

Abstract: The restoration of marker-occluded hematoxylin and eosin (H&E) stained whole slide histology images is a critical task in digital pathology, as annotations and markings made by pathologists often obscure important tissue structures. This work proposes a deep learning-based approach utilizing Generative Adversarial Networks (GANs) to automatically reconstruct and restore occluded regions in histopathological images. The model is trained on paired datasets of clean and artificially occluded H&E images to learn the underlying tissue distribution and generate realistic reconstructions. The generator network predicts the missing regions, while the discriminator ensures the authenticity and structural consistency of the restored output. The proposed method effectively removes artifacts such as pen marks and labels while preserving cellular morphology and diagnostic features. Experimental results demonstrate improved visual quality and structural similarity compared to traditional inpainting techniques, making it a promising solution for enhancing the reliability of digital pathology workflows.

Keywords: Generative Adversarial Networks (GANs), Histopathology Image Restoration, Hematoxylin and Eosin (H&E) Staining, Whole Slide Imaging (WSI), Image Inpainting, Marker Occlusion Removal, Digital Pathology, Deep Learning, Medical Image Processing, Tissue Structure Preservation, Image Reconstruction, Computer-Aided Diagnosis (CAD),Biomedical Image Analysis, Artifact Removal.

INTRODUCTION: It is a common practice for pathologists to annotate regions of interest, such as tumor, directly on the glass slide to which the tissue sample was affixed. These annotations are useful for tasks at the macro level such as tumor detection and routine cancer diagnosis. Though the rise of powerful commercial scanners coupled with advanced image viewers has enabled widespread slide digitization, many legacy slides are still scanned with the pathologist's original hand-drawn annotations. Such annotations often occlude important details of the image, preventing implementation of recent digital pathology workflows at the micro level. For example, on-going research has shown the significance of the tumor micro-environment on cancer progression and treatment, specifically in the field of immuno-oncology [1, 2]. The identification, localization, and spatial relationships of certain immune cells with tumor cells hold valuable prognostic potential for personalized treatment regimens [3]. However, tasks such as nuclei segmentation and classification, and the extraction of features and predictive biomarkers in the following steps cannot be accurately conducted without first producing an occlusion-free image. CycleGAN was introduced in 2017 [4] for unpaired image translation tasks, in which the training images in the source and target domains do not need to correspond to one another. This method uses cycle consistency to avoid mode collapse, which is the transformation of all input images in the source domain to one or a few images in the target domain. Through adding a second generator convolutional neural network (CNN), CycleGAN ensures that the individual information of each image is

maintained throughout the transformation by reconstructing the original image from the output. CycleGAN is typically good at translating the texture of the input to match the target while not altering the structure significantly. This has motivated many applications for CycleGAN including digital pathology, where it has been used for data augmentation and style transfer. Fu et al. [5] used this model to transform artificial nuclei segmentation masks to synthetic nuclei fluorescence images, thus producing a large annotated dataset of nuclei required for training a nuclei segmentation CNN. Mahmood et al. [6] developed a similar approach for generating training datasets for nuclei segmentation in hematoxylin and eosin stained (H&E) images. Additionally, they trained a CycleGAN to imitate nuclei segmentation that was performed by human experts. Shaban et al. [7] showed that CycleGAN outperforms state-of-the-art methods for stain normalization, in which the goal is to eliminate the image variations resulting from different imaging parameters such as equipment and environment. Xu et al. [8] took it a step further and used CycleGAN for transforming H&E images into immunohistochemistry images in order to take advantage of possibilities that these images provide.

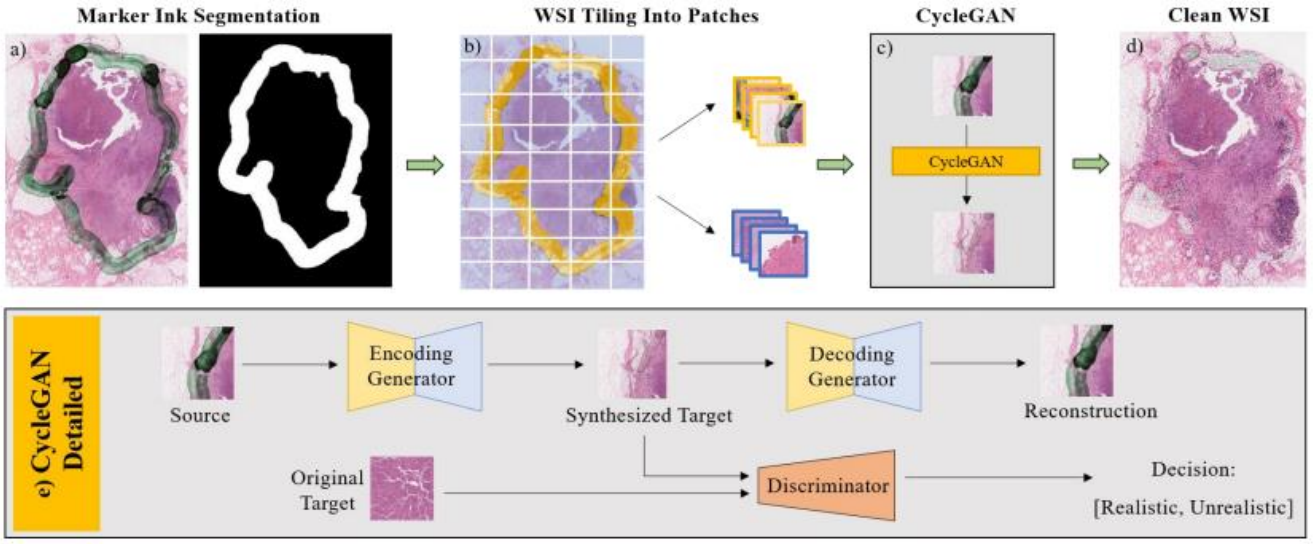

Fig. 1. The pipeline employed for training the model

H&E images to clean ones. We treat this as a style transfer problem and train a CycleGAN with up to 300 whole slide images (WSI) to remove the marker ink (Figure 1). We show the quality of the results by performing a blind test once by a human expert and once by a separately trained deep residual network. We also demonstrate the fidelity of our results by conducting a morphological test of the results. Finally, we process a sample of the reconstructed WSIs and attain an increase of up to 94,000 detected nuclei per slide.

DATA PREPARATION AND TRAINING: We surveyed an internal dataset of 1,100 H&E stained WSIs from human melanoma tissues. In 305 of these images, markers were used to delineate the tumor border with colors black, green, and blue (250, 50, and 5 WSIs respectively.) In 170 of the images, the intensity of the ink made the underlying tissue visually imperceptible. Therefore, we divided the data into four categories (Figure 2): black (80), blue (5), green (50), and opaque (170) . None of the WSIs contained annotations with more than one marker ink color. We trained two models using two different training sets. In the first one, we aimed for data balance by handpicking 12

WSIs (three from each category). In the second dataset we maximized data diversity by increasing the number of WSIs to 300, introducing an imbalance where 80% of the occluded images contained black marker ink. In each case, 5 of the WSIs were set aside for testing, with two slides from the black and one from every other category. The marker region in each of the WSIs was segmented using HistoQC toolkit [9] and the segmentations were care

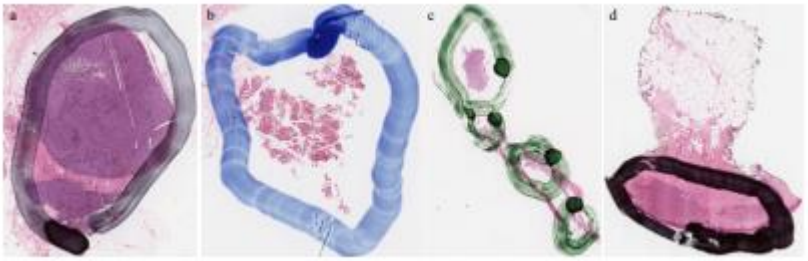

Fig. 2. Dataset was divided into 4 categories based on marker ink color and transparency: a) black, b) blue, c) green, and d) opaque.

fully corrected in ImageScope software (Aperio, ImageScope version 12.4). Training and testing patches of size 128x128 pixels were then extracted at random locations. Any patch with partial or full marker regions was considered a marker patch, while clean patches lacked any amount of marker ink. The patches from the empty background of the WSIs were included in the dataset to steer the model to learn the removal of marker ink rather than generating tissue, when the marker image was totally opaque. However, the number of background patches was maintained under 25% of the total clean patches. The total number of patches in either training dataset was 250,000 with half of them being marker patches. CycleGAN is composed of two generative and one discriminative CNNs, which are trained adversarially. One of the generative CNNs is trained to the remove marker ink by outputting a patch that is similar enough to a clean tissue to mislead the discriminate CNN, which is trained in detecting the originally clean patches from those output by the generative CNN. The second generative CNN is trained to reconstruct the input using the output of the first CNN. Although, this synthetic marker patch is not used, this process ensures the preservation of the visual information individual to each input patch. Originally, CycleGAN failed to converge due to the discriminative CNN overpowering the generative ones, thus depriving them of the gradient information they need to adapt to an improving discriminative model. To remedy this, we changed the discriminative optimizer from Adam to stochastic gradient descent with a learning rate of 0.0001. Adam was used for the generative models with a learning rate of 0.0002. No decay was applied to the learning rates. The training was done from scratch for 150 epochs with a batch size of 64 patches on a Nvidia Quadro P6000 GPU. In the testing phase, when a reconstruction of the whole slide was needed, it was divided into 128x128 patches and each patch including marker ink was input to the generative network separately and then stitched together to reconstruct the original WSI (Figure 3). To avoid the resulting checkerboard alias, these patches were chosen at a stride of 100 pixels and the intensity of the overlapping pixels was averaged. The total number of patches processed for the 5 slides was 2,000,000.

VALIDATION:

Our goal in this work was to correct as much of the marker regions as possible while: (1) maintaining the tissue structure underneath the marker; and (2) ensuring that the corrected regions look indistinguishable from uncontaminated H&E regions to the downstream human- or computer-guided analysis. We designed four validation

experiments to quantify the fulfillment of the aforementioned goals. To measure the success of our method in transforming the marker regions into clean H&E, we had the corrected results tested against uncontaminated tissue once by a classifier CNN and once manually. The manual blind test was performed by an H&E image quality control specialist in our organization. 100 patches of size 500x500 pixels were randomly extracted from the test set of 5 WSIs, where half of the patches were clean tissue and the rest corrected marker tissue regions. The expert was then asked to discern which of the patches were corrected and which ones uncontaminated originally. To test the similarity of the clean and the corrected regions, we also used a binary classifier CNN. A ResNet [10] with 50 layers was trained on 124,000 clean and marker image patches with a validation and test size of both 41,000 patches. The patches were extracted from the same 12 WSIs used in training the CycleGAN as the aforementioned strategy. The training was performed for 100 epochs with a batch size of 128 patches with a learning rate of 0.0001 and an Adam optimizer. To test the similarity of the corrected patches to the uncontaminated ones, 100 corrected non-background patches were chosen from the reconstructed test set of 5 WSIs and fed to the CNN. Ideally, the corrected patches look identical to the clean ones and are classified as clean tissue by the CNN. Therefore, the percentage of marker patches classified as clean was considered as a success measure of our method. Historically, CycleGAN excels at translating image texture while keeping the structure intact. However, we needed to confirm that as the marker trace in the images is removed, the boundary of the nuclei is not altered. To test the fidelity of the reconstructed images, we randomly sampled 120 of the test patches, 30 from each category. An alteration of the nuclei and other tissue borders would manifest itself through discrepancy of edge information in the two images. To measure edge similarity, we calculated the correlation of image gradient magnitudes for each input and output image patch. The purpose of correcting H&E images for marker is to recover the information covered by marker ink. To assess the efficacy of our method, a nuclei segmentation algorithm was designed in Definiens Tissue Studio 4.4.2 software (Definiens AG, Munich) and the number of segmented nuclei was counted in the test set of WSIs before and after correction.

RESULTS:

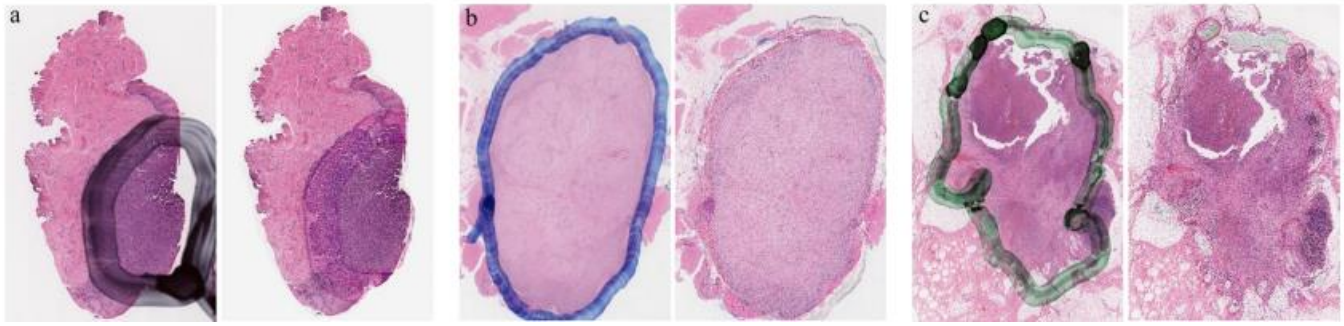

Fig. 3. Marker occluded whole slide images and reconstruction output for categories black (a), blue (b), and green (c)

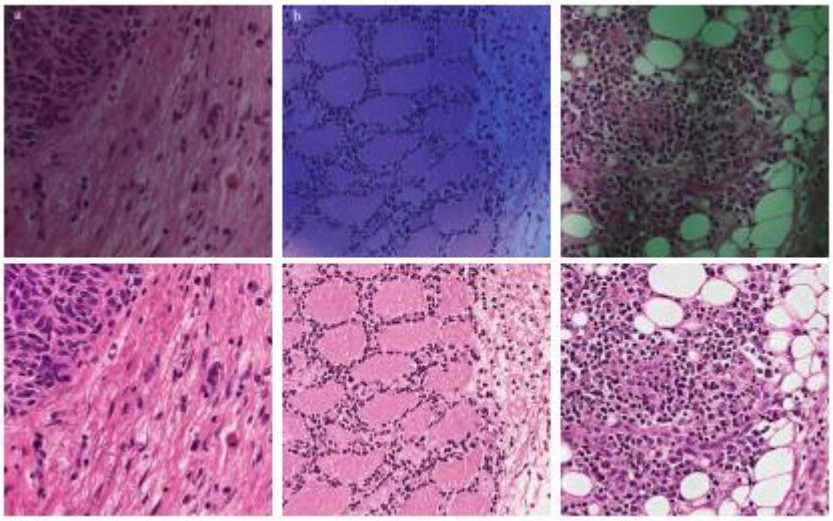

Fig. 4. Marker occluded patches (top row) and reconstruction results (bottom row) for black (a), blue (b), and green (c)

Advantages

- Effectively removes marker occlusions without manual intervention
- Preserves fine-grained tissue structures and cellular details
- Produces high-quality, realistic image reconstructions
- Reduces dependency on clean datasets in pathology workflows
- Enhances performance of downstream AI-based diagnostic models
- Faster and more scalable compared to manual correction methods

Applications

- Digital pathology and histopathological image analysis
- Preprocessing for AI-based cancer detection systems
- Archival restoration of annotated medical datasets
- Biomedical research involving tissue morphology analysis
- Telepathology and remote diagnosis systems
- Medical image enhancement for training datasets

Conclusion: This study presents an efficient GAN-based framework for restoring marker-occluded regions in H&E stained whole slide images. The approach successfully reconstructs missing tissue information while maintaining structural integrity and visual realism. By leveraging adversarial learning, the model outperforms conventional image restoration techniques in terms of accuracy and perceptual quality. The restored images can support improved diagnostic analysis and downstream computational pathology tasks. Overall, this method contributes to enhancing the usability of annotated histopathology datasets and facilitates better clinical decision-making.

Future Scope: Integration with real-time pathology imaging systems, Extension to multi-stain and multiplexed histological images, Development of unsupervised or self-supervised GAN models, Incorporation of attention

mechanisms for improved localization, Deployment in clinical decision support systems, Enhancement with explainable AI for interpretability. Optimization for large-scale whole slide image processing.

FUTURE SCOPE: Real-Time Clinical Deployment: Developing lightweight and optimized architectures for real-time restoration in digital pathology workflows and hospital systems. Multi-Artifact Removal: Extending the system to handle multiple artifacts simultaneously such as blur, folds, bubbles, and staining inconsistencies in whole slide images (WSIs). 3D Histopathological Reconstruction: Future work can focus on 3D tissue reconstruction from restored 2D slices for better tumor analysis and surgical planning.

REFERENCES:

1. B. Venkatesh, T. Shah, A. Chen, and S. Ghafurian, "Restoration of marker occluded hematoxylin and eosin stained whole slide histology images using generative adversarial networks," *arXiv preprint arXiv:1910.06428*, 2019.
2. R. Rong *et al.*, "Enhanced pathology image quality with Restore–Generative Adversarial Network," *The American Journal of Pathology*, vol. 193, no. 4, pp. 404–416, 2023.
3. M. Ali *et al.*, "Generative adversarial networks in digital pathology and histopathological image processing: A review," *Journal of Pathology Informatics*, 2021.
4. Z. He, J. He, J. Ye, and Y. Shen, "Artifact restoration in histology images with diffusion probabilistic models," *MICCAI*, 2023.
5. S. Butte, H. Wang, A. Vakanski, and M. Xian, "Enhanced Sharp-GAN for histopathology image synthesis," *IEEE International Symposium on Biomedical Imaging (ISBI)*, 2023.
6. M. Ali, M. Hussain, and D. Koundal, "Generative adversarial networks for medical image processing: Recent advancements," *Archives of Computational Methods in Engineering*, 2025.
7. A. Rana, G. Yauney, A. Lowe, and P. Shah, "Computational histological staining and destaining of prostate biopsy images using GANs," *arXiv preprint arXiv:1811.02642*, 2018.
8. T. Abraham *et al.*, "Slide-free MUSE microscopy to H&E histology modality conversion using GANs," *arXiv preprint arXiv:2008.08579*, 2020.
9. S. Butte, H. Wang, M. Xian, and A. Vakanski, "Sharpness loss regularized GAN for histopathology image synthesis," in *Proc. IEEE Int. Symp. Biomedical Imaging (ISBI)*, 2022, pp. 1–5.
10. S. Butte, H. Wang, A. Vakanski, and M. Xian, "Enhanced Sharp-GAN for histopathology image synthesis," in *Proc. IEEE Int. Symp. Biomedical Imaging (ISBI)*, 2023.
11. R. Rong, S. Wang, X. Zhang, Z. Wen, X. Cheng, L. Jia, D. M. Yang, Y. Xie, X. Zhan, and G. Xiao, "Enhanced pathology image quality with Restore–Generative Adversarial Network," *The American Journal of Pathology*, vol. 193, no. 4, pp. 404–416, 2023.
12. Y. Chai, B. Xu, K. Zhang, N. Lepore, and J. Wood, "MRI restoration using edge-guided adversarial learning," *IEEE Access*, vol. 8, pp. 83858–83870, 2020.
13. M. Ali, M. Hussain, and D. Koundal, "Generative adversarial networks for medical image processing: Recent advancements," *Archives of Computational Methods in Engineering*, vol. 32, no. 2, pp. 1185–1198, 2025.
14. Y. Zhou, F. Jin, G. Suo, et al., "ResViT-GANNet: A deep learning framework for classifying breast cancer histopathology images using GAN-based augmentation," *BMC Medical Imaging*, vol. 25, 2025.

15. D. Mahapatra, B. Bozorgtabar, J.-P. Thiran, and L. Shao, "Structure preserving stain normalization of histopathology images using self-supervised semantic guidance," *arXiv preprint arXiv:2008.02101*, 2020.
16. U. Upadhyay and S. Awate, "A mixed-supervision multilevel GAN framework for image quality enhancement," *arXiv preprint arXiv:2106.15575*, 2021.
17. M. M. Ho, S. Dubey, Y. Chong, B. Knudsen, and T. Tasdizen, "F2FLDM: Latent diffusion models with histopathology pre-trained embeddings for image restoration," *arXiv preprint arXiv:2404.12650*, 2024.
18. M. Ali *et al.*, "Generative adversarial networks in digital pathology and histopathological image processing: A review," *Journal of Pathology Informatics*, vol. 12, 2021.
19. Y. Zhang, H. Xie, S. Zhuang, and X. Zhan, "Image restoration and optimization based on GAN models," *Discover Applied Sciences*, 2026.
20. "Advancement in image restoration through GAN-based approach," in *IEEE Conference Publication*, IEEE Xplore, 2024.